Quaternary Research (2017), **88**, 1–13.

doi:10.1017/qua.2017.24

High precision U/Th dating of the rock paintings at Mt. Huashan, Guangxi, southern China

Qing-Feng Shao[a]*, Edwige Pons-Branchu[b], Qiu-Ping Zhu[c], Wei Wang[d], Hélène Valladas[b], Michel Fontugne[b]

[a]Key Laboratory of Virtual Geographic Environment (Nanjing Normal University), Ministry of Education, Nanjing 210023, China
[b]Laboratoire des Science du Climat et de l'Environment, LSCE/IPSL, CEA-CNRS-UVSQ, Université Paris Saclay, Gif-Sur-Yvette F-91198, France
[c]Cultural Relics Management Institution of Ningming County, Guangxi Zhuang Autonomous Region, Ningming 532500, China
[d]Guangxi Museum of Nationalities, Guangxi Zhuang Autonomous Region, Nanning 530028, China

(Received September 20, 2016; Accepted February 14, 2017)

Abstract

The rock art and the associated natural scenery at 38 sites located in the Zuojiang River valley, in the southwest of Guangxi Zhuang Autonomous Region, southern China, were inscribed recently on UNESCO's World Heritage List. The painted panel at the site of Mt. Huashan is probably the largest known rock art panel in the world, consisting of approximately 1900 identifiable figures and occupying an area of approximately 8000 m^2. To determine a precise age on the rock art at Mt. Huashan, 56 secondary carbonate layers above and below the paintings were studied for their mineralogy, oxygen, and carbon isotopic compositions and dated by the ^{230}Th/U method. The ^{230}Th/U dating results demonstrate that ages of the rock paintings can be bracketed between 1856 ± 16 and 1728 ± 41 yr BP corresponding to the middle to the end of the Eastern Han dynasty (AD 25 to 220). The results imply that the rock painting practices at Mt. Huashan probably lasted more than a century, and the Zuojiang rock art is younger than that at Baiyunwan and Cangyuan in Yunnan Province by 1 to 10 centuries.

Keywords: High precision U/Th dating; Secondary carbonates; World Heritage; Mt. Huashan rock paintings; Zuojiang River valley

INTRODUCTION

The Zuojiang River, originating in the mountainous area of northern Vietnam, flows some 450 km through the southwest part of Guangxi Zhuang Autonomous Region (GZAR), southern China. The Zuojiang River valley is characterized by a subtropical karst landform developed on a Carboniferous to Triassic limestone. This valley is renowned for the numerous red paintings preserved on steep cliffs along the Zuojiang River and its tributaries, namely the Lijiang, Mingjiang, and Heishui rivers (Fig. 1). Joint investigations of the rock paintings organized during the 1950s and 1980s by Chinese researchers, including geologists, archaeologists, historians, ethnologists, and art scientists, documented approximately 80 rock art sites stretching for more than 200 km (Qin et al., 1987). The paintings are all drawn with ocher in a very similar style and range from 10 to 130 m above the active river surface. The motifs include mostly human figures, animals (e.g., horses, dogs, and birds), objects (e.g., boats, bells, drums, knives, and swords), and some designs probably representing the sun. The rock art at 38 sites, along with the surrounding rivers, terraces, and karstic mountains, forms the unique "Zuojiang Huashan Rock Art Cultural Landscape", which was placed on UNESCO's World Heritage List in 2016 (Fig. 1). Among these rock art sites, Mt. Huashan is the most spectacular, noted for the large scale and high density of motifs and excellent preservation (Huashan is called *pay laiz* in the local language, which literally means "a mountain with colorful paintings").

The rock paintings in the Zuojiang River valley are widely believed to have been created between the Warring States period and the Eastern Han dynasty (475 BC to AD 220) on the basis of the comparison of the objects depicted (such as bronze drums, goat horn–shaped bells, and ring-head knives) with the archaeological findings from ancient tombs in southern and southwestern China (Qin et al., 1987). The paintings are commonly attributed to the Luo Yue people, who are believed to be the ancestors of the Zhuang nationality and who inhabited this valley and the neighboring areas across present China and Vietnam from the Shang dynasty to the Han dynasty (1600 BC to AD 220) according to ancient documents (Qin et al., 2015).

*Corresponding author at: Key Laboratory of Virtual Geographic Environment (Nanjing Normal University), Ministry of Education, Nanjing 210023, China. E-mail: qingfengshao@njnu.edu.cn (Q.-F. Shao).

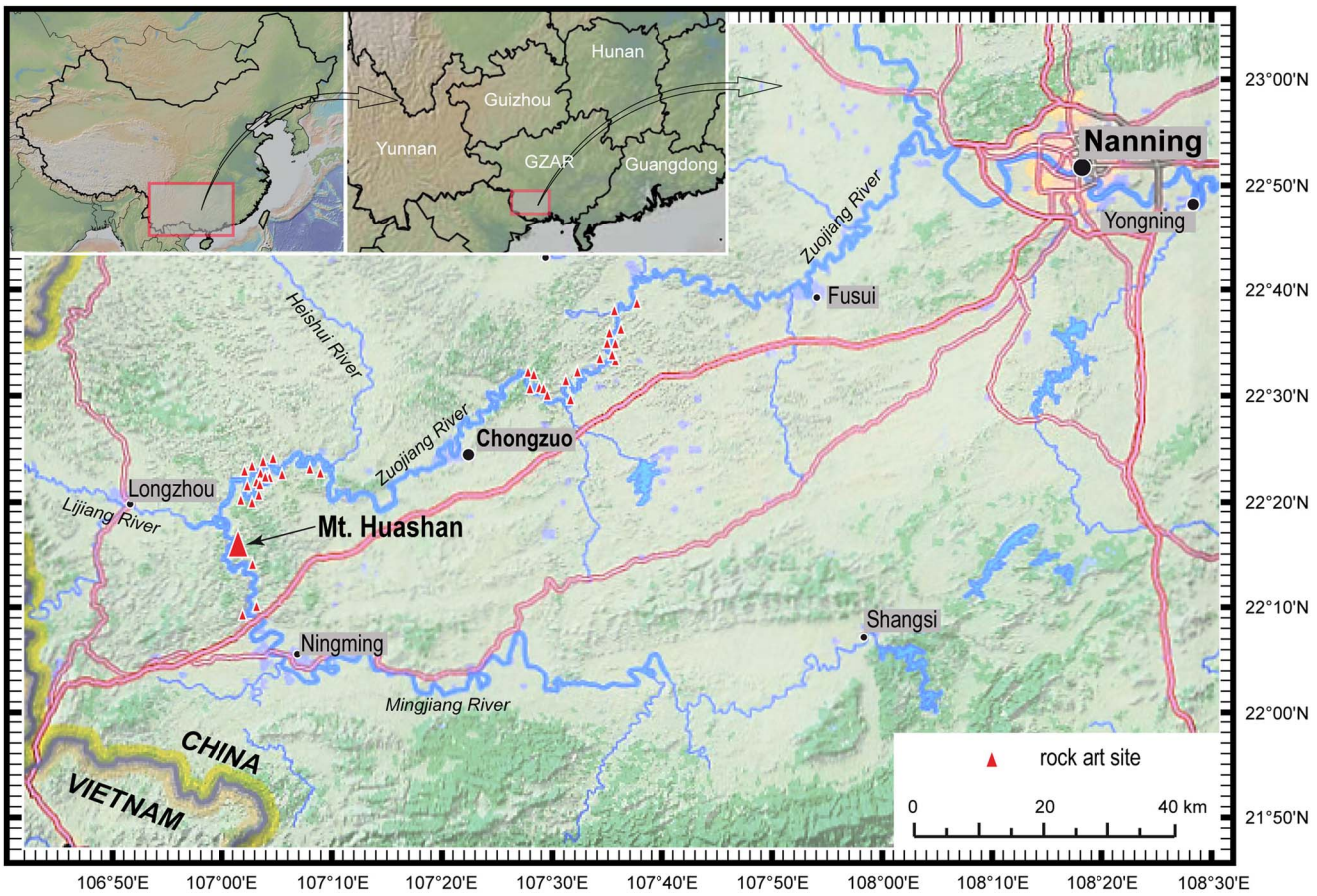

Figure 1. (color online) Location of the 38 rock art sites in the "Zuojiang Huashan Rock Art Cultural Landscape" on the World Heritage List.

These ancient paintings provide a precious record of the social life and religious beliefs of the Luo Yue people.

However, to determine a precise age on rock art is usually difficult because of the lack of stratigraphic context and datable material. When the pigment contains organic material, accelerator mass spectrometry (AMS) ^{14}C dating can be used to date the paintings directly with less than 1 mg of carbon for analysis (e.g., Russ et al., 1990; Valladas et al., 1990, 1992, 2001; Watchman, 1993; Steelman et al., 2002; Cole and Watchman, 2005; Smith et al., 2009; Morwood et al., 2010; David et al., 2013; Quiles et al., 2016). Alternatively, thin carbonate layers overlying or underlying the artwork can be used to establish the minimum or maximum age for the rock art by the ^{230}Th/U method using thermal ionization mass spectrometry or multiple-collector inductively coupled plasma mass spectrometry (MC-ICP-MS) techniques, which require a very small amount of sample for analysis (10 to ~100 mg) (e.g., Pike et al., 2005, 2012; Aubert et al., 2007, 2014; Garcia-Diez et al., 2013; Hellstrom and Pickering, 2015). Nevertheless, secondary carbonate precipitates on the surface of bedrock, subjected to runoff over time, may experience postdepositional U migration (i.e., open system behavior). The coupled ^{230}Th/U and AMS ^{14}C approach allows the presumption of a closed system for the carbonates to be tested and thus is increasingly used in rock art dating studies (e.g., Plagnes et al., 2003; Taçon et al., 2012; Fontugne et al., 2013; Pons-Branchu et al., 2014a; Corchón et al., 2015).

The Zuojiang rock paintings were made exclusively with red ocher without any organic pigment that could be used for AMS ^{14}C dating. Fortunately, many paintings at the Mt. Huashan site are overlain by carbonate precipitates. They provide a great opportunity to date the rock art by the ^{230}Th/U dating method. Yuan et al. (1986) attempted to date these secondary carbonates using ^{14}C with a liquid scintillation counting technique, and they constrained the rock art age to between 2370 and 2115 yr BP. Because of the limited number of samples and uncertainties in ^{14}C age corrections, however, the authors pointed out that the real age range could extend from the Spring and Autumn period to the Eastern Han dynasty (770 BC to AD 220).

To determine a precise age on the rock paintings at the Mt. Huashan site, the present study carried out high-precision ^{230}Th/U dating of 56 carbonate samples associated with the paintings. The AMS ^{14}C method was applied on 9 of the samples dated by ^{230}Th/U to test their respective reliability and consistency. The high-precision ^{230}Th/U dating results are discussed in light of X-ray diffraction (XRD), stable isotope (δ^{18}O and δ^{13}C), and AMS ^{14}C analyses to assess the reliability of the chronology.

https://doi.org/10.1017/qua.2017.24 Published online by Cambridge University Press

MATERIALS AND METHODS

Rock paintings at Mt. Huashan

The Zuojiang River valley is on the fringes of the Yunnan-Guizhou Plateau to the northwest. This is a karstic area surrounded by isolated limestone hills, karst peaks, vast plains, and a complex of drainage systems. The hills are generally less than 500 m above sea level (m asl), and the plains vary from 80 to 200 m asl with multiple terraces (Qin et al., 1987). The Zuojiang River valley has a subtropical monsoon climate with an annual average temperature of ~22°C and rainfall of ~1250 mm.

The Mt. Huashan site (22°15.70′N, 107°00.61′E) is located on the bank of the Mingjing River about 20 km northwest of Ningming County, GZAR (Fig. 2). The painted cliff at Mt. Huashan is approximately 350 m long and 270 m high and is oriented north to south, leaning slightly forward over the Mingjing River. The painted panel is about 170 m wide and between 30 and 90 m above the river surface, covering an area of approximately 8000 m^2. Although it has suffered from severe erosion, more than 1900 images are identifiable (Qin et al., 1987). Human figures account for approximately 75% of the images; they are commonly 30 to 300 cm high, depicted in frontal or side view, in a semisquatting posture with the arms raised from the elbow. The typical grouping of the human figures is one large frontal human figure in the center surrounded by several smaller human figures. The large frontal human figure wears decorated headgear, carries weapons at the waist (such as a knife or sword), and has an animal at his feet (such as a dog), whereas the smaller human figures do not have decorations or weapons.

This rock art site was registered among the important units of cultural relics under national protection by the state council in 1988, was placed on the tentative World Heritage List of China by the state administration of cultural heritage in 2007, and became a World Heritage Site in 2016.

Samples

Mt. Huashan is composed of Carboniferous limestone and covered by evergreen shrubs. Because of the moist monsoon climate and subtropical vegetation, dissolution and precipitation processes here are very active. As rainwater percolates down through the soil, it is enriched with CO_2 forming a weak carbonic acid, owing to respiration and organic decomposition. The acidic water, with a high partial pressure of CO_2, dissolves the bedrock along the rock fractures. At various places on the limestone cliff, the water discharges from the bedrock, which causes degassing of CO_2 and precipitation of secondary carbonates. Refer to White (1988) and Ford and Williams (2007) for detailed descriptions of the karst processes.

Secondary carbonates for ^{230}Th/U dating were collected between the years 2013 and 2014 and benefited from the handrails that were built for a rock art conservation project, which make it possible to access all of the painted area.

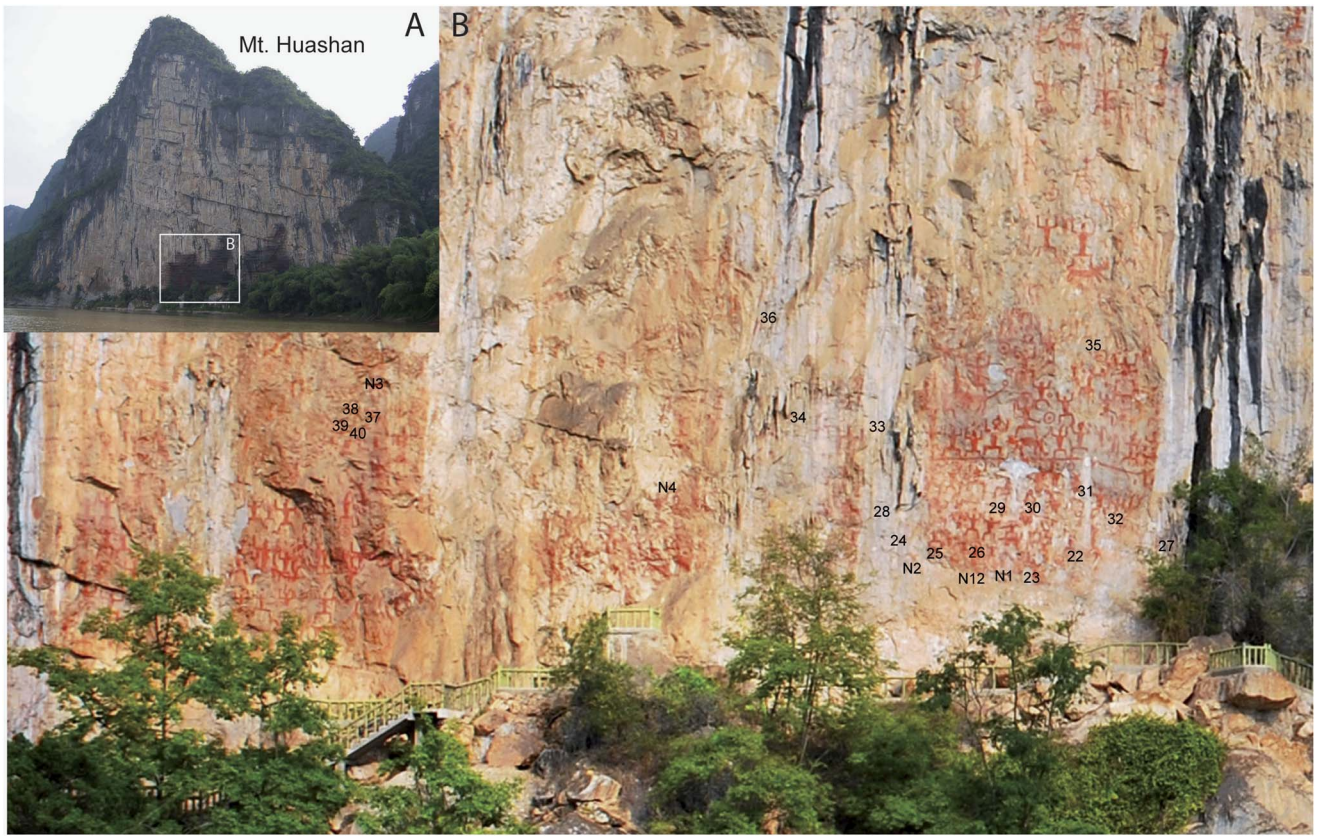

Figure 2. (color online) (A) Mt. Huashan. (B) Part of the rock paintings; the numbers correspond to sample location.

https://doi.org/10.1017/qua.2017.24 Published online by Cambridge University Press

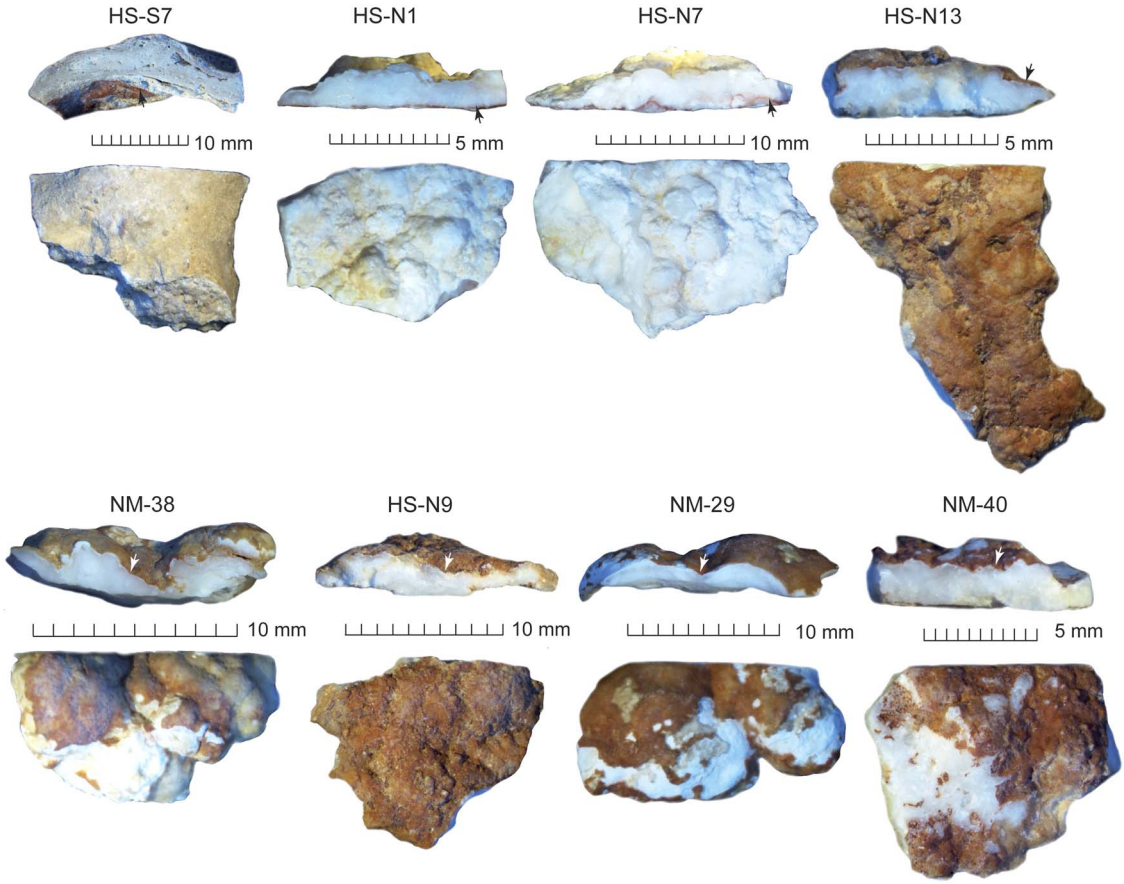

Figure 3. (color online) Photos of the representative samples from Mt. Huashan. Samples of HS-S7, HS-N1, and HS-N7 are above the pigment layer; samples of HS-N13, NM-38, HS-N9, NM-29, and NM-40 are below the pigment layer. The arrows point to the pigment layer.

Only secondary carbonates that have a clear stratigraphic relationship with the rock art were sampled, including 34 samples overlying the paintings and 22 samples underlying the paintings (Fig. 3, Supplementary Table 1, and Supplementary Fig. 1). In addition, 2 bedrock samples were collected. In order to minimize the damage to the paintings, all samples were taken in a diameter less than 2 cm.

Methods

Located on the surface of the bedrock, the paintings, like the overlying calcite deposits, have been exposed to intense weathering. Preliminary analyses were performed on the carbonate samples to be dated by ^{230}Th/U to characterize their nature and formation process.

Mineral and stable isotope ($\delta^{18}O$, $\delta^{13}C$) analyses

Aliquots of the samples collected from the Mt. Huashan site were analyzed by XRD in order to evaluate the mineralogy and to assist in the interpretation of isotopic values. The XRD analysis was performed on powdered samples using a Rigaku D/max 2500VL/PC XRD. The diffraction patterns ($2\theta = 6° - 95°$) were recorded at room temperature using Cu $K_{\alpha 1}$ radiation ($\lambda = 1.5406$ Å) at a scanning speed of 5°/min and a step size of 0.02° (2θ). Diffraction patterns were matched using the International Center for Diffraction Data (ICDD, 2500) database.

The samples analyzed by XRD were recovered and submitted for measurements of isotopic compositions of oxygen and carbon using a Thermo-Finnigan MAT-253 mass spectrometer fitted with an online automated preparation system (Kiel Carbonate Device III). Samples were calibrated against the international calcite standard NBS-19 and were reported in per mil relative to the Vienna Pee Dee belemnite (VPDB) standard. Repeated measurements of this standard display an analytical precision of typically 0.08‰ (1σ).

AMS ^{14}C analysis

Nine samples (aliquots of carbonate grains prepared for ^{230}Th/U dating) were used to the AMS ^{14}C analysis: five were prepared and analyzed by the Laboratoire de Mesure du Carbone 14 (LMC14) laboratory, Gif-sur-Yvette Laboratoire des Science du Climat et de l'Environment (LSCE) and Accélérateur pour la Recherche en sciences de la Terre, Environnement, Muséologie Installé à Saclay (ARTEMIS) AMS national facilities, in Saclay, France, and four at the Beta Analytic radiocarbon dating laboratory in Miami, USA. At LSCE, the samples were finely crushed and washed in

https://doi.org/10.1017/qua.2017.24 Published online by Cambridge University Press

distilled water using an ultrasonic bath. The grains were then lightly etched using 0.01N HNO_3 and rinsed with distilled water. Under vacuum, the carbonate was reacted with phosphoric acid, and the evolved CO_2 was reduced to obtain graphite targets prepared following the method described by Tisnérat-Laborde et al. (2001). Results are expressed as conventional ages following Stuiver and Polach (1977). The sample treatment and AMS measurement protocols used in the Beta Analytic laboratory are available on their website (http://www.radiocarbon.com).

^{230}Th/U dating

The secondary carbonate pieces were mechanically cleaned by a dental drill to remove the yellowish surface layer and attached pigment. They were then gently crushed into small grains less than 5 mm in size and ultrasonically cleaned in 18.2 MΩ ultrapure water. The pure and well-crystallized grains were handpicked for ^{230}Th/U dating.

The samples (n = 42) collected in 2014 were analyzed at Nanjing Normal University. The clean samples (50–200 mg) were weighed and dissolved in 7N HNO_3 in a Teflon beaker containing a known quantity of a ^{229}Th-^{233}U-^{236}U triple spike. After sample dissolution, $HClO_4$ (~30 µL) was added to decompose organic material. The sample-spike mixture was heated on a hot plate overnight to equilibrate. U and Th were then separated from each other and from other cations by passing the sample solution through a U-TEVA resin column according to Douville et al. (2010). Sample matrix elements were first eliminated by rinsing with 3N HNO_3. Subsequently, Th was eluted using 3N HCl, and finally, U was eluted using 1N HCl. $HClO_4$ (~30 µL) was added again to the sample solutions to remove the organics dropped off from the U-TEVA resins. The U and Th fractions were then dried and diluted in a mixture of 0.5N HNO_3 and 0.01N HF for U and Th isotopic analysis.

The U and Th isotopic measurements were carried out on a Neptune MC-ICP-MS. U was measured statically by ^{233}U, ^{235}U, ^{236}U, and ^{238}U on Faraday cups and ^{234}U simultaneously on a secondary electron multiplier (SEM). Th was analyzed with ^{230}Th and ^{229}Th alternately on the SEM and ^{232}Th on a Faraday cup. The U isotopic ratios of the HU-1 standard, which is a commonly used uraninite standard at secular radioactive equilibrium, were measured before and after every U and Th isotopic measurement for samples. Mass fractionation was corrected by comparing the measured ^{238}U/^{235}U to the value of 137.760 for the HU-1 standard and to the value of 137.818 for natural samples (Hiess et al., 2012) with an exponential law (Russell et al., 1978). The mass fractionation for U and Th are assumed to be equivalent. The yield of SEM to Faraday cup was assessed by the δ^{234}U measured in the HU-1 standard. Hydride interferences, machine abundance sensitivity, and amplifier gains were evaluated every day prior to sample measurements.

The samples (n = 14) collected in 2013 were prepared at the LSCE laboratory and analyzed on a Neptune plus MC-ICP-MS fitted with a jet pump interface. The procedure used for U/Th chemical separation and isotopic measurement is detailed in Pons-Branchu et al. (2014b).

^{230}Th/U ages were calculated using half-lives of 75,584 yr and 245,620 yr for ^{230}Th and ^{234}U, respectively (Cheng et al., 2013). The ^{230}Th/U age uncertainty was estimated by Monte-Carlo simulations with consideration of all sources of analytical uncertainty.

RESULTS

Mineralogy and stable isotopes

The results of XRD analysis on the secondary carbonates, bedrock, and pigment are presented in Table 1 and Figure 4. The XRD analysis on the secondary carbonates showed that 33 samples contain pure calcite, 2 are made of aragonite, and 21 are a mixture of aragonite with calcite and/or hydromagnesite [$Mg_5(CO_3)_4(OH)_2(H_2O)_4$]. XRD analysis on the 2 bedrock samples identified calcite and dolomite. The red pigment attached on the surface of sample NM-40 (Fig. 3) was carefully scraped off using a sharp blade. The XRD spectrum of this pigment shows the presence of hematite (Fe_2O_3), quartz, and calcite (Fig. 4). This analysis confirms the previous XRD analysis: the major color-generating element is Fe_2O_3, but calcite, quartz, and kaolin are also present, indicating that the pigment was derived from natural red ocher mixed with clay (Guo et al., 2010).

The results of oxygen and carbon isotopic analyses on these carbonates are presented in Table 1 and Figure 5. Overall, the data show a strong positive correlation between the δ^{18}O and δ^{13}C values, with correlation coefficients of 0.34 for the aragonitic samples, 0.66 for the calcitic samples, and 0.77 for all of the data (except for the HS-S3 sample). It can also be observed that the aragonitic samples are more enriched in both ^{18}O and ^{13}C compared with the calcitic ones. The δ^{18}O values in the aragonitic samples range from –5.94‰ to –2.83‰ and have a mean of –4.76‰, whereas in the calcitic samples they vary from –9.37‰ to –4.48‰ with a mean of –6.66‰, except for the HS-S3 sample, which is extremely depleted in ^{18}O with a δ^{18}O value of –16.70‰. The distribution of δ^{13}C values is in the range of –1.03‰ to +3.49‰ for the aragonitic samples and in the range of –9.71‰ to +2.02‰ for the calcitic samples. Oxygen and carbon isotopic analyses on the two bedrock samples yielded consistent results with a mean of –6.59‰ for δ^{18}O and +2.68‰ for δ^{13}C, which are in the typical δ^{18}O and δ^{13}C value ranges for Carboniferous marine limestone and dolomite (Veizer et al., 1999).

These mineralogical and isotopic results show that the secondary carbonate layers associated with the paintings are present as different mineralogical phases and are likely to have different chronologies and/or chemical behavior.

^{230}Th/U dating results

A summary of the MC-ICP-MS U/Th analytical results completed on the 56 samples is presented in Table 1. The aragonitic and calcitic samples are distinguishable in

https://doi.org/10.1017/qua.2017.24 Published online by Cambridge University Press

Table 1. Results of X-ray diffraction (XRD), stable isotope, and U-series analyses on the samples from Mt. Huashan rock art site.

Sample	Stratigraphy	Type XRD[a]	$\delta^{18}O$ [‰]	$\delta^{13}C$ [‰]	Laboratory code	^{238}U [ppm]	^{232}Th [ppb]	$\delta^{234}U$ [‰]	($^{230}Th/^{238}U$)	($^{230}Th/^{232}Th$)	U/Th age [yr][b]	$\delta^{234}U_i$ [‰]	Corrected age [yr BP][c]
NM-1	Overlying	Calcite	–6.18	–0.09	NNU-379	3.418 ± 0.007	24.628 ± 0.063	22.4 ± 2.4	0.00264 ± 0.00005	1.15 ± 0.02	282 ± 5	22.4 ± 2.4	23 ± 89
NM-2	Overlying	Calcite	–6.79	–2.27	NNU-380	2.215 ± 0.002	19.138 ± 0.059	53.1 ± 1.3	0.00400 ± 0.00006	1.45 ± 0.02	415 ± 6	53.2 ± 1.3	117 ± 118
NM-3	Overlying	Calcite	–5.91	–1.10	NNU-381	2.998 ± 0.003	61.315 ± 0.304	45.8 ± 1.2	0.00660 ± 0.00007	0.99 ± 0.01	690 ± 7	45.8 ± 1.2	109 ± 217
NM-5	Overlying	Calcite	–6.15	–0.08	NNU-382	2.917 ± 0.006	19.400 ± 0.052	36.5 ± 2.1	0.00285 ± 0.00004	1.33 ± 0.02	300 ± 4	36.5 ± 2.1	51 ± 90
NM-6	Overlying	Calcite	–6.03	0.09	NNU-383	2.329 ± 0.003	12.112 ± 0.033	155.4 ± 1.5	0.00778 ± 0.00005	4.67 ± 0.03	736 ± 5	155.7 ± 1.5	543 ± 65
NM-7	Overlying	Calcite	–4.48	1.42	NNU-384	3.166 ± 0.021	7.975 ± 0.061	–46.8 ± 6.6	0.00141 ± 0.00004	1.72 ± 0.05	161 ± 5	–46.8 ± 6.6	21 ± 39
NM-9	Overlying	Calcite	–6.57	–0.37	NNU-385	3.210 ± 0.006	16.750 ± 0.045	122.6 ± 2.5	0.00217 ± 0.00004	1.30 ± 0.02	211 ± 4	122.6 ± 2.5	15 ± 64
NM-11	Overlying	Calcite	–6.13	–2.80	NNU-386	2.096 ± 0.003	7.577 ± 0.008	21.6 ± 0.6	0.00787 ± 0.00006	6.62 ± 0.05	843 ± 7	21.6 ± 0.6	675 ± 52
NM-14	Overlying	Calcite	–6.50	–2.56	NNU-389	2.495 ± 0.009	10.819 ± 0.047	152.7 ± 3.2	0.00197 ± 0.00004	1.42 ± 0.03	187 ± 4	152.8 ± 3.2	16 ± 53
NM-16	Overlying	Calcite	–6.35	–3.49	NNU-387	2.301 ± 0.003	15.643 ± 0.053	87.9 ± 1.6	0.00513 ± 0.00007	2.34 ± 0.03	515 ± 7	87.9 ± 1.6	272 ± 92
NM-19	Overlying	Calcite	–5.16	1.17	NNU-390	3.091 ± 0.006	17.201 ± 0.043	75.6 ± 2.1	0.00571 ± 0.00007	3.20 ± 0.03	581 ± 8	75.7 ± 2.1	369 ± 75
NM-20	Overlying	Calcite	–6.37	–4.25	NNU-391	2.544 ± 0.005	25.378 ± 0.055	40.9 ± 1.6	0.00724 ± 0.00007	2.26 ± 0.02	761 ± 8	40.9 ± 1.6	423 ± 141
NM-21	Overlying	Calcite	–5.80	–3.80	NNU-313	2.903 ± 0.006	8.769 ± 0.053	115.2 ± 2.3	0.01896 ± 0.00017	19.82 ± 0.11	1869 ± 17	115.8 ± 2.3	1729 ± 41
NM-22	Overlying	Aragonite	–5.36	–0.01	NNU-392	2.840 ± 0.003	22.455 ± 0.101	242.7 ± 1.5	0.00547 ± 0.00006	2.17 ± 0.02	481 ± 5	242.9 ± 1.5	236 ± 91
NM-23	Overlying	Ara./dol.	–4.36	5.78	NNU-393	4.396 ± 0.032	19.088 ± 0.154	376.3 ± 8.7	0.00256 ± 0.00006	1.84 ± 0.06	203 ± 5	376.6 ± 8.7	50 ± 45
NM-25	Overlying	Aragonite	–4.42	0.78	NNU-395	3.561 ± 0.006	12.521 ± 0.049	391.0 ± 2.4	0.00267 ± 0.00004	2.38 ± 0.04	209 ± 3	391.2 ± 2.4	74 ± 36
NM-26	Overlying	Ara./cal.	–5.17	0.07	NNU-396	3.066 ± 0.006	12.650 ± 0.068	179.6 ± 2.3	0.00324 ± 0.00004	2.45 ± 0.03	299 ± 4	179.7 ± 2.4	136 ± 51
NM-30	Overlying	Ara./cal.	–5.48	–0.48	NNU-423	3.089 ± 0.005	8.125 ± 0.018	331.3 ± 2.6	0.00274 ± 0.00003	3.25 ± 0.03	225 ± 2	331.4 ± 2.6	105 ± 29
NM-31	Overlying	Ara./cal.	–5.13	–0.20	NNU-424	2.441 ± 0.003	11.297 ± 0.038	190.6 ± 1.5	0.00293 ± 0.00004	1.98 ± 0.03	269 ± 4	190.7 ± 1.5	94 ± 55
NM-32	Overlying	Ara./dol.	–5.58	1.78	NNU-425	2.862 ± 0.005	4.819 ± 0.008	221.2 ± 2.3	0.00246 ± 0.00003	4.59 ± 0.05	220 ± 3	221.3 ± 2.3	116 ± 20
NM-33	Overlying	Ara./cal.	–4.99	–1.03	NNU-426	2.885 ± 0.004	25.198 ± 0.043	314.0 ± 2.4	0.00403 ± 0.00004	1.45 ± 0.01	335 ± 3	314.1 ± 2.4	82 ± 94
NM-37	Overlying	Calcite	-	-	NNU-134	4.098 ± 0.017	9.669 ± 0.100	92.2 ± 4.7	0.00549 ± 0.00006	7.23 ± 0.06	549 ± 7	92.3 ± 4.7	423 ± 32
NM-39	Overlying	Ara./cal.	–4.09	3.57	NNU-136	3.907 ± 0.019	4.777 ± 0.032	172.9 ± 4.9	0.00202 ± 0.00003	5.15 ± 0.06	188 ± 3	173.0 ± 4.9	94 ± 15
HS-N1	Overlying	Ara./hyd.	–5.58	0.45	LSCE-4252	2.673 ± 0.006	5.062 ± 0.003	270.7 ± 0.9	0.00639 ± 0.00002	11.61 ± 0.03	550 ± 2	271.1 ± 0.9	448 ± 19
HS-N2	Overlying	Ara./hyd./cal.	–5.15	0.29	LSCE-4250	3.098 ± 0.017	3.523 ± 0.002	434.9 ± 0.8	0.02213 ± 0.00005	69.13 ± 0.06	1696 ± 4	437.0 ± 0.8	1614 ± 12
HS-N3	Overlying	Ara./hyd.	–5.73	2.61	LSCE-4240	3.803 ± 0.012	6.597 ± 0.004	178.9 ± 0.8	0.00290 ± 0.00001	6.37 ± 0.02	269 ± 1	179.0 ± 0.8	171 ± 17
HS-N4	Overlying	Ara./hyd.	–5.38	3.27	LSCE-4241	3.353 ± 0.018	4.379 ± 0.004	372.9 ± 0.7	0.00736 ± 0.00003	18.12 ± 0.03	587 ± 2	373.5 ± 0.7	496 ± 13
HS-N7	Overlying	Ara./hyd.	–3.11	1.64	LSCE-4242	2.177 ± 0.007	4.904 ± 0.004	180.6 ± 0.6	0.00618 ± 0.00002	9.67 ± 0.03	573 ± 2	180.9 ± 0.6	462 ± 25
HS-N10	Overlying	Ara./hyd.	–3.40	2.31	LSCE-4238	3.338 ± 0.013	2.074 ± 0.002	318.2 ± 0.6	0.00900 ± 0.00003	45.87 ± 0.10	748 ± 3	318.9 ± 0.6	671 ± 7
HS-N11	Overlying	Calcite	–6.28	–1.71	LSCE-4244	3.567 ± 0.019	3.582 ± 0.003	54.8 ± 0.6	0.00356 ± 0.00002	11.57 ± 0.02	369 ± 2	54.9 ± 0.6	279 ± 13
HS-N12	Overlying	Ara./hyd.	–4.06	–0.25	LSCE-4245	2.886 ± 0.014	2.652 ± 0.003	360.3 ± 0.7	0.01240 ± 0.00004	42.58 ± 0.07	1000 ± 4	361.3 ± 0.7	918 ± 10
HS-S1	Overlying	Calcite	–6.38	–1.98	LSCE-4248	1.447 ± 0.010	15.992 ± 0.014	46.1 ± 0.8	0.00633 ± 0.00002	2.46 ± 0.01	663 ± 2	46.2 ± 0.8	379 ± 109
HS-S5	Overlying	Calcite	–5.96	–0.43	LSCE-4237	2.374 ± 0.006	11.337 ± 0.010	52.1 ± 0.8	0.00976 ± 0.00004	6.45 ± 0.01	1017 ± 5	52.3 ± 0.8	825 ± 64
HS-S7	Overlying	Calcite	–9.21	–9.71	NNU-317	0.387 ± 0.001	0.760 ± 0.001	76.0 ± 0.8	0.01724 ± 0.00018	26.70 ± 0.27	1761 ± 18	76.3 ± 0.8	1646 ± 32
NM-4	Underlying	Calcite	–7.34	–7.96	NNU-428	0.444 ± 0.001	0.616 ± 0.001	137.3 ± 0.7	0.11472 ± 0.00039	257.20 ± 0.91	11,570 ± 42	141.9 ± 0.7	11,471 ± 46
NM-8	Underlying	Calcite	–7.11	–2.91	NNU-306	0.772 ± 0.003	11.031 ± 0.064	52.7 ± 3.4	0.07437 ± 0.00070	16.37 ± 0.09	7985 ± 84	53.9 ± 3.5	7539 ± 210
NM-10	Underlying	Calcite	–6.77	–5.27	NNU-307	0.497 ± 0.001	1.401 ± 0.008	117.0 ± 2.8	0.04807 ± 0.00057	53.00 ± 0.44	4793 ± 59	118.6 ± 2.8	4657 ± 70
NM-12	Underlying	Calcite	–8.32	–4.61	NNU-308	0.700 ± 0.001	21.854 ± 0.097	143.6 ± 1.5	0.06868 ± 0.00110	6.94 ± 0.09	6746 ± 111	146.0 ± 1.6	5912 ± 412
NM-13	Underlying	Calcite	–9.37	–6.47	NNU-309	1.515 ± 0.002	17.104 ± 0.076	134.1 ± 1.1	0.04506 ± 0.00032	12.57 ± 0.06	4418 ± 33	135.7 ± 1.1	4073 ± 147
NM-15	Underlying	Calcite	–7.29	–2.42	NNU-310	1.130 ± 0.001	22.818 ± 0.126	95.3 ± 1.2	0.04092 ± 0.00076	6.33 ± 0.09	4149 ± 79	96.2 ± 1.3	3556 ± 274
NM-17	Underlying	Calcite	–7.05	–3.09	NNU-311	2.548 ± 0.005	18.109 ± 0.077	66.0 ± 1.6	0.02501 ± 0.00018	11.10 ± 0.07	2588 ± 19	66.4 ± 1.6	2338 ± 94
NM-18	Underlying	Calcite	–5.62	–1.72	NNU-312	3.379 ± 0.007	7.359 ± 0.033	57.6 ± 2.1	0.03150 ± 0.00022	45.63 ± 0.23	3296 ± 24	58.1 ± 2.2	3175 ± 38
NM-24	Underlying	Calcite	–6.99	–3.08	NNU-421	1.006 ± 0.001	35.318 ± 0.072	139.7 ± 1.5	0.24445 ± 0.00066	21.68 ± 0.04	26,193 ± 88	150.1 ± 1.7	25,253 ± 447

Table 1. (*Continued*)

Sample	Stratigraphy	Type XRD[a]	$\delta^{18}O$ [‰]	$\delta^{13}C$ [‰]	Laboratory code	^{238}U [ppm]	^{232}Th [ppb]	$\delta^{234}U$ [‰]	$(^{230}Th/^{238}U)$	$(^{230}Th/^{232}Th)$	U/Th age [yr][b]	$\delta^{234}U_i$ [‰]	Corrected age [yr BP][c]
NM-27	Underlying	Calcite	–6.83	–4.80	NNU-314	0.233 ± 0.001	1.421 ± 0.002	144.5 ± 1.3	0.03283 ± 0.00038	16.49 ± 0.19	3172 ± 37	145.7 ± 1.3	2953 ± 88
NM-28	Underlying	Calcite	–3.87	1.19	NNU-422	1.607 ± 0.002	11.926 ± 0.029	159.8 ± 1.5	0.14422 ± 0.00042	60.39 ± 0.15	14,437 ± 50	166.4 ± 1.6	14,190 ± 104
NM-29	Underlying	Ara./hyd.	–5.12	0.75	NNU-398	4.722 ± 0.019	2.645 ± 0.016	461.9 ± 5.1	0.02570 ± 0.00017	141.95 ± 0.75	1932 ± 15	464.4 ± 5.2	1858 ± 16
NM-34	Underlying	Calcite	–6.91	–2.54	NNU-315	1.093 ± 0.001	26.342 ± 0.111	163.5 ± 1.1	0.10389 ± 0.00101	13.50 ± 0.10	10,178 ± 103	168.0 ± 1.1	9527 ± 308
NM-35	Underlying	Calcite	–6.09	–8.76	NNU-130	0.339 ± 0.001	16.594 ± 0.079	–17.2 ± 2.7	0.62986 ± 0.00372	40.27 ± 0.11	112,180 ± 1321	–23.7 ± 3.7	110,679 ± 1506
NM-36	Underlying	Calcite	–8.51	–3.65	NNU-427	1.634 ± 0.002	10.248 ± 0.019	106.4 ± 1.4	0.10533 ± 0.00037	52.57 ± 0.13	10,892 ± 42	109.7 ± 1.4	10,667 ± 90
NM-38	Underlying	Ara./cal.	–2.83	3.49	NNU-135	2.846 ± 0.013	10.476 ± 0.119	145.5 ± 3.7	0.02637 ± 0.00031	22.24 ± 0.14	2538 ± 32	146.5 ± 3.7	2382 ± 56
NM-40	Underlying	Ara./cal.	–5.94	1.33	NNU-137	4.375 ± 0.019	6.902 ± 0.037	174.8 ± 4.4	0.02464 ± 0.00020	48.53 ± 0.27	2310 ± 21	176.0 ± 4.5	2208 ± 28
HS-N9	Underlying	Ara./hyd./cal.	–5.24	0.38	NNU-138	3.753 ± 0.005	2.990 ± 0.060	228.0 ± 1.8	0.02382 ± 0.00014	91.42 ± 1.92	2135 ± 13	229.3 ± 1.8	2052 ± 19
HS-N13	Underlying	Ara./hyd.	–4.73	0.03	LSCE-4249	2.638 ± 0.008	4.312 ± 0.005	389.4 ± 1.0	0.03327 ± 0.00011	64.74 ± 0.07	2644 ± 9	392.3 ± 1.0	2547 ± 19
HS-S2	Underlying	Calcite	–6.90	–2.70	LSCE-4254	0.296 ± 0.001	1.823 ± 0.001	110.4 ± 0.5	0.24081 ± 0.00034	121.26 ± 0.10	26,583 ± 43	119.0 ± 0.6	26,360 ± 89
HS-S3	Underlying	Calcite	–16.70	2.02	LSCE-4239	0.087 ± 0.001	12.100 ± 0.011	66.2 ± 0.8	0.81088 ± 0.00086	17.87 ± 0.01	152,111 ± 437	101.8 ± 1.2	148,385 ± 1883
HS-S6	Underlying	Calcite	–5.88	–1.87	LSCE-4247	2.462 ± 0.008	8.053 ± 0.006	39.0 ± 0.9	0.02764 ± 0.00006	29.62 ± 0.03	2944 ± 7	39.4 ± 1.0	2800 ± 40

[a]The type XRD of Ara./hyd./cal./dol. is a mixture of aragonite, hydromagnesite, calcite, and/or dolomite. The analytical errors were given at the 2σ level.
[b]U/Th ages were calculated with the decay constants of $\lambda_{230} = 9.1705 \times 10^{-6}$/yr and $\lambda_{234} = 2.82206 \times 10^{-6}$/yr (Cheng et al., 2013). The U/Th ages were corrected with assumption of the initial $^{230}Th/^{232}Th$ atomic ratio of $4.4 \pm 2.2 \times 10^{-6}$, a value for a material at secular equilibrium, with the bulk earth $^{232}Th/^{238}U$ value of 3.8 and with an assumed error of 50%.
[c]The corrected ages are given at the "BP" scale, before AD 1950.

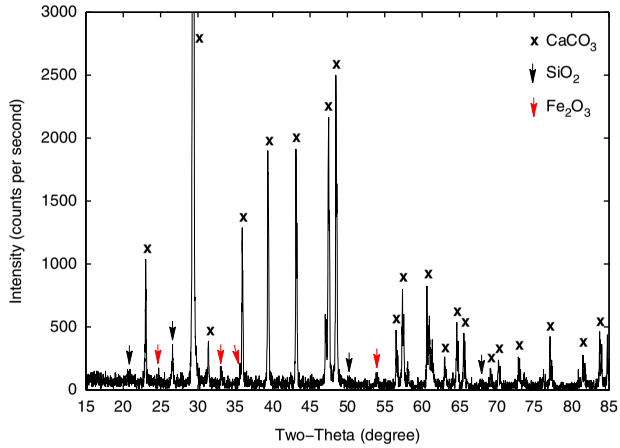

Figure 4. (color online) X-ray diffraction spectrum of the pigment sample (NM-40) from Mt. Huashan rock art site.

U concentration and U isotopic compositions. The average U concentration is 3.20 μg/g in the aragonitic samples and 1.94 μg/g in the calcitic ones. The measured $\delta^{234}U$ values range from 145.5‰ to 461.9‰ with a mean of 277.1‰ in the aragonitic samples, and from –46.8‰ to 163.5‰ with a mean of 81.4‰ in the calcitic samples.

The average ^{232}Th concentration is 8.6 pg/g in the aragonitic samples and 14.8 pg/g in the calcitic samples. The measured ^{232}Th implies the presence of at least some ^{230}Th when the carbonates were formed. The present-day $^{230}Th/^{232}Th$ activity ratios are as low as 1 in the young samples, whereas values as high as 250 were measured in the old ones. Correction for initial ^{230}Th was made for each sample on the assumption of an initial $^{230}Th/^{232}Th$ atomic ratio of $4.4 \pm 2.2 \times 10^{-6}$ (or activity ratio of 0.82 ± 0.41),

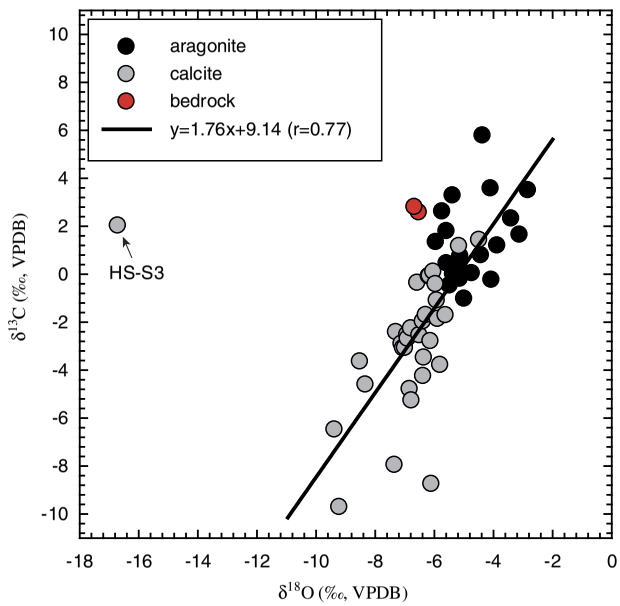

Figure 5. (color online) Plot of $\delta^{18}O$ against $\delta^{13}C$ measured in the samples from Mt. Huashan rock art site. VPDB, Vienna Pee Dee belemnite.

https://doi.org/10.1017/qua.2017.24 Published online by Cambridge University Press

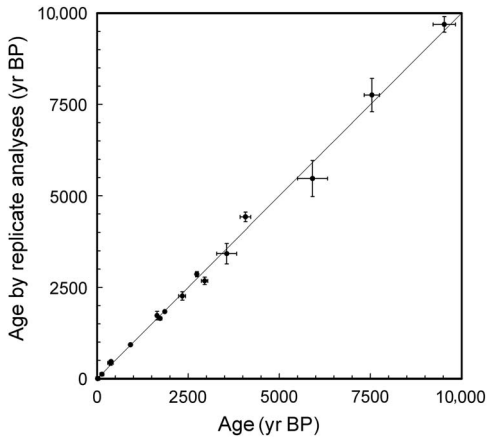

Figure 6. Comparison of the U/Th ages by replicate analyses for the Holocene samples from Mt. Huashan rock art site. The x-axis corresponds to the U/Th ages used in main text (Table 1); the y-axis corresponds to the ages by replicate analyses (Supplementary Table 2).

which is a value for a material assumed to be at secular equilibrium for ^{230}Th, ^{234}U, and ^{238}U, with the bulk crustal ^{232}Th/^{238}U concentration ratio of 3.8 ± 1.9.

The samples overlying the paintings have corrected ages in the range of 1728 ± 41 to 14 ± 64 yr BP (before AD 1950), and the samples underlying the paintings are between 1856 ± 16 and 148,385 ± 1883 yr BP. Replicate U/Th analyses on 19 samples found slight differences in U concentration and isotopic compositions (Supplementary Table 2), but the ^{230}Th/U ages are consistent (Fig. 6), indicating that these samples behaved as closed systems with respect to uranium.

AMS ^{14}C results

Radiocarbon values are reported in Table 2 as conventional age (using Oxcal 4.2 software [Ramsey, 2009]; ages reported at 95.4% confidence interval) after normalization to δ^{13}C of 25‰; they were corrected for backgrounds (accelerator analysis and chemical treatment) and isotopic fractionation using the δ^{13}C measured during the AMS analysis (Stuiver and Polach, 1977). Ages are widely scattered, ranging from 1290 ± 30 to 38,910 ± 630 ^{14}C yr BP. Calibrated ages using the IntCal 13 (Reimer et al., 2013) are also reported, which represent the ages assuming no dead carbon within the samples. They range between 1180 cal yr BP (sample HS-S1) and ca. 44,000 cal yr BP (sample HS-S3), the latter being at the limit of the method. The ^{230}Th/U ages allow calculations of the dead carbon percentage (DCP) values (Genty et al., 1999) for the paired U/Th and ^{14}C analysis (Table 2). These DCP values are unusually high with a mean of 31.5% and values up to 57.4%, with generally higher values obtained for aragonitic samples.

DISCUSSION

Stable isotopes

The mechanism for sample deposition in open-air or well-ventilated sites such as $CaCO_3$ layers on shelter or tufas could be different from speleothems in caves. Ihlenfeld et al. (2003) and Garnett et al. (2004) found that tufa can be deposited in conditions close to isotopic equilibrium between $CaCO_3$ and water for oxygen and carbon. In contrast, Lojen et al. (2009) observed that isotopic composition of tufas can be largely influenced by nonequilibrium precipitation, which favors the incorporation of isotopically depleted C and O into the carbonate.

In Mt. Huashan samples, isotopic equilibrium between $CaCO_3$ and waters could not be verified. The δ^{18}O and δ^{13}C data are not used here for paleoclimatic studies, but in order to constrain the origin of calcitic samples (primary or neomorphic), as the mechanism for this transformation could be similar in different environments (including caves and open-air sites).

Data on both calcitic and aragonitic samples follow the same O/C trend (Fig. 5). The main difference in the O and C isotopic composition between the two minerals is that δ^{18}O and δ^{13}C values are generally higher within aragonitic samples than in calcitic ones (Fig. 7).

In a previous study on speleothems, Zhang et al. (2014) highlighted that the aragonite/calcite transformation alters the δ^{18}O signal (with lower δ^{18}O values for secondary calcite), but not the δ^{13}C. In another case, Woo and Choi (2006) found

Table 2. ^{14}C dating results and calculated dead carbon percentage (DCP) for the samples from Mt. Huashan rock art site. XRD, X-ray diffraction.

Laboratory code	Sample name	Type-XRD	Conventional age (yr BP, ±2σ)	^{14}C age (0% DCP, cal yr BP)	U-Th corrected age (yr BP, ±2σ)	DCP (%)
GifA 13362	HS-N7	Aragonite/ hydromagnesite	5210 ± 30	6095–5909	462 ± 25	45.3
GifA 13363	HS-N12	Aragonite/ hydromagnesite	4880 ± 30	5657–5586	918 ± 10	38.6
GifA 13364	HS-N2	Aragonite/ hydromagnesite/ calcite	6010 ± 30	6941–6756	1614 ± 12	41.4
GifA 13365	HS-S3	Calcite	38,910 ± 630	43,989–42,010	148,385 ± 1883	-
GifA 13366	HS-S1	Calcite	1290 ± 30	1286–1180	379 ± 109	11.3
Beta-399678	NM-29	Aragonite/ hydromagnesite	8730 ± 30	9885–9557	1858 ± 16	57.4
Beta-399677	NM-18	Calcite	4150 ± 30	4825–4577	3175 ± 38	13.3
Beta-399676	NM-17	Calcite	6570 ± 30	7558–7427	2338 ± 94	41.3
Beta-399675	HS-S7	Calcite	2040 ± 30	2111–1904	1646 ± 32	3.5

https://doi.org/10.1017/qua.2017.24 Published online by Cambridge University Press

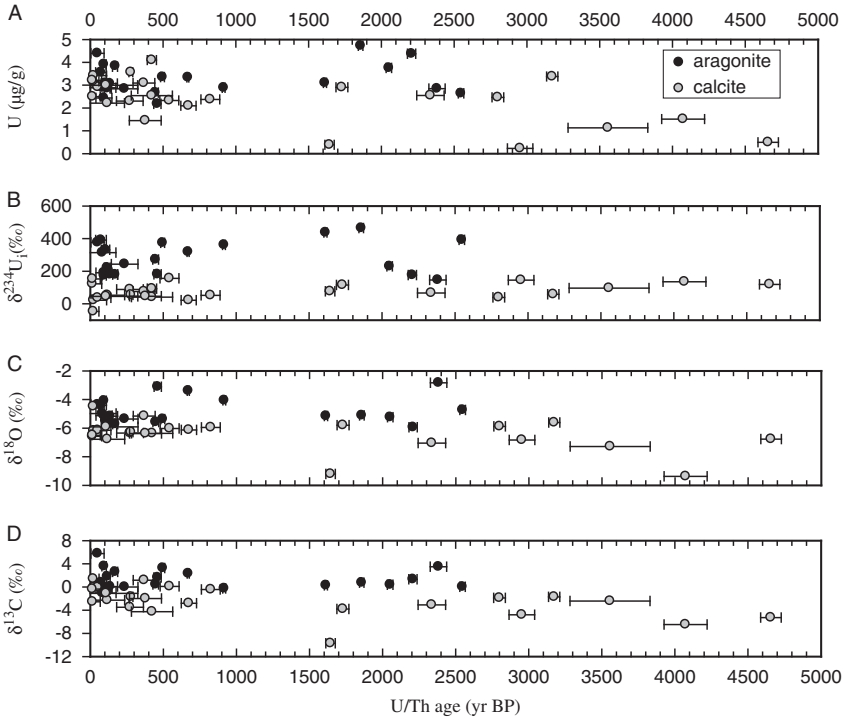

Figure 7. Comparison of aragonitic and calcitic samples in terms of U concentration (A), initial $\delta^{234}U$ (B), $\delta^{18}O$ (C), and $\delta^{13}C$ (D), plotted against sample age.

that the $\delta^{18}O$ and $\delta^{13}C$ values of neomorphic calcite are similar to the isotopic composition of primary aragonite. They also observed that unaltered aragonite speleothems are enriched in ^{13}C with respect to the primary calcitic speleothems. They argued that this could indicate a stronger limestone imprint and/or a higher soil water component. A similar conclusion was reached by McMillan et al. (2005) during their study of two speleothems from Clamouse Cave (France): they reported higher $\delta^{18}O$ and $\delta^{13}C$ values in aragonitic layers than in primary calcite within the same speleothems.

Following these studies, the higher $\delta^{18}O$ and $\delta^{13}C$ values observed in Mt. Huashan aragonitic samples than in calcitic ones provide further evidence of the original calcitic samples, with a strong host rock imprint within aragonitic samples. At this site, the mechanism proposed for the deposition of aragonite involves strong water/host rock interaction with limestone dissolution in closed conditions (low exchange with the atmosphere) leading to high $\delta^{13}C$ and DCP values. This mechanism is strengthened by the high $\delta^{234}U$ composition in the aragonitic samples (Fig. 7), which is higher in dry periods or regions because of the longer interaction time between water and host rock compared with wetter periods or regions (e.g., Kaufman et al., 1998; Ayalon et al., 1999; Hellstrom and McCulloch, 2000; Robinson et al., 2004; Zhou et al., 2005; Göktürk et al., 2011; Maher et al., 2014). In contrast, the low $\delta^{13}C$, $\delta^{18}O$, DCP, and $\delta^{234}U$ values determined for calcitic samples indicate lower water/host rock interaction, congruent dissolution of the host rock (lower $\delta^{234}U$, closer to equilibrium), and higher CO_2 exchange with the atmosphere (resulting in lower DCP). The development of both minerals on the same cliff could be because of the existence of two water pathways, one within rock fractures close to the cliff surface (relatively rapid water transfer in the case of calcite formation) and another within interstitial pore spaces (slower water transfer in the case of aragonite).

Reliability of the ^{230}Th/U ages

Open system behavior for the ^{230}Th/U chronometer could result in U gain or loss, but in the case of speleothems or thin calcitic and/or aragonitic layers, the most common phenomenon is U loss (e.g., Railsback et al., 2002; Plagnes et al., 2003), leading to anomalously old ^{230}Th/U ages (Pons-Branchu et al., 2014a; Hellstrom and Pickering, 2015). In addition, the initial ^{230}Th introduced by detrital materials can also make apparent ^{230}Th/U age older than the true age. For ^{14}C dating, an open system behavior is expected to introduce young C producing apparent ^{14}C ages that are too young (e.g., Holmgren et al., 1994; Goslar et al., 2000).

As aragonite is a metastable mineral, its transformation to calcite is commonly observed. This transformation within speleothems and secondary carbonates could result in U loss and thus a possible age bias toward an apparent age that is older than the real age (e.g., Ortega et al., 2005; Lachniet et al., 2012). Thus, the validity of the ^{230}Th/U dating on the calcitic samples relies on their origin: primary calcite (i.e., not produced by aragonite transformation) can yield reliable ^{230}Th/U ages, whereas neomorphic calcite (derived from

https://doi.org/10.1017/qua.2017.24 Published online by Cambridge University Press

aragonite transformation) could result in erroneous ages. McDermott et al. (1999) and McMillan et al. (2005) observed for two speleothems primary calcitic and aragonitic layers within the two stalagmites, deposited during a brief dry period. Aragonite and calcite can therefore be deposited in the same karstic context.

For the coupled ^{230}Th/U and ^{14}C analysis, excluding HS-S3, which is at the ^{14}C dating limit, the ^{14}C ages are systematically older than ^{230}Th/U ages (Table 2). The difference between the two chronometers is most likely because of the presence of dead carbon (nonatmospheric carbon, originating from soil and bedrock), and not to an open system behavior or uncorrected detrital Th contamination, which would result in older ^{230}Th/U ages. In the present study, the comparison of ^{230}Th/U and ^{14}C results validates the ^{230}Th/U ages on the aragonitic samples and underlines an unusually large DCP within these samples that could be because of closed system calcareous dissolution and/or the presence of old organic matter (Noronha et al., 2014). This comparison also indicates that the ^{230}Th/U ages of the calcitic samples may be reliable, and the DCP fraction deduced from ^{14}C analysis is within the range of classical values for speleothems (3.5% to 13.5% for the three samples HS-S1, HS-S7, and NM-18, and 41.3% for NM-17).

The general convergence of the ages obtained by the two methods (^{14}C and ^{230}Th/U) suggests a chemically closed system, allowing the validation of ages. For Huashan carbonates, the ^{14}C and ^{230}Th/U ages do not converge; nevertheless, ^{14}C activities suggest that the system has remained chemically closed.

The age of the rock paintings

So far, the antiquity of rock art in China has not been widely studied with absolute dating methods. Using ^{14}C dating of carbonates, the age of Mt. Huashan rock paintings has been estimated to be between 2370 and 2115 cal yr BP (Yuan et al., 1986), and the paintings at Cangyuan, Yunnan Province, were dated to between 3100 and 2960 yr BP (Wang, 1984; Bednarik and Li, 1991). However, these ^{14}C ages are likely too old because of the DCP input. Recently, ^{230}Th/U and ^{14}C dating methods were applied to a flowstone formed above and below a large painted deer at Baiyunwan, Yunnan Province, and yielded a maximum age of 5740 cal yr BP and a minimum ^{230}Th/U age of 2050 cal yr BP for the rock art (Taçon et al., 2012).

From the motifs of bronze drums, goat horn–shaped bells, and ring-head knives in the Mt. Huashan rock paintings, an indirect age between the Warring States period and the Eastern Han dynasty (475 BC to AD 220) can be inferred from comparison with the objects excavated from ancient tombs in southern and southwestern China (Qin et al., 1987). In the present study, the 56 calcitic/aragonitic samples yielded ^{230}Th/U ages ranging from 148,385 ± 1883 cal yr BP to 14 ± 64 yr BP. The age distribution shows that the number of analyzed samples generally increases toward recent times, and there is an apparent gap between 1600 yr BP and 920 yr BP (Fig. 8A). This time interval generally corresponds to a weakening monsoon event centered around 1600 yr BP in East Asia, according to a stalagmite δ^{18}O record from the Dongge Cave (Fig. 8B; Wang et al., 2005), approximately 350 km northwest of the Mt. Huashan site. It also corresponds to a distinct China-wide cold period between 1720 and 1150 yr BP, revealed by multiple paleoclimate proxy records including ice cores, tree rings, lake sediments, and historical documents (Yang et al., 2002). Beyond sampling bias, the absence of samples in this age gap probably is related to the relatively dry and cold climate, which may have suppressed the formation of secondary carbonates on the cliff. On the other hand, the large number of samples dated to the past 200 yr BP may correspond to the strengthening monsoon and the increasing temperature since roughly AD 1800 (Fig. 8B; Yang et al., 2002; Wang et al., 2005).

The ^{230}Th/U dating in combination with mineral, stable isotopic, and ^{14}C analyses on these carbonate samples strongly indicate that the aragonitic samples were formed in a closed carbonate system and that the calcitic samples were formed in a relatively open condition. These analyses do not show evidence of open system behavior after carbonate precipitation. Therefore, the ^{230}Th/U ages obtained are able to represent the age of the mineral formation. Accordingly, the maximum age of the rock paintings can be estimated to be 1856 ± 16 yr BP or AD 94 ± 16 (by NM-29, the youngest of the samples underlying the paintings), and the minimum age can be estimated to be 1728 ± 41 cal yr BP or AD 222 ± 41 (by NM-21, the oldest of the samples overlying the paintings), corresponding to the middle to the end of the Eastern Han dynasty (AD 25 to AD 220).

CONCLUSIONS

The XRD analyses show that the secondary carbonates formed on the painted cliff at the Mt. Huashan site can be separated generally into calcitic (>55%) and aragonitic (~40%) varieties. Isotopic (δ^{18}O, δ^{13}C, and ^{14}C) and ^{230}Th/U analyses on these carbonate samples did not exhibit clear evidence of postdepositional chemical alteration. Based on the ^{230}Th/U ages, the age of the Mt. Huashan rock paintings can be bracketed between 1856 ± 16 and 1728 ±41 yr BP, corresponding to the middle to the end of the Eastern Han dynasty (AD 25 to 220), and possibly even to the early part of the Three States period (AD 220 to 280), considering the uncertainties in ^{230}Th/U ages. The results suggest that the rock painting practices lasted probably more than 1 century in the Mt. Huashan site, and that this rock art is younger than that at Baiyunwan and Cangyuan in Yunnan Province by 1 to 10 centuries according to the available numerical dating results. This study also shows that the indirect dating of rock art using secondary carbonate deposits over- or underlying paintings may produce a large range of ages, sometimes far away from the age of the painting itself. Because the delay between the carbonate formation and the rock art practice remains unknown, dating of a large number of samples, as performed in this study, may be necessary to constrain the timing of rock art by the U/Th dating

https://doi.org/10.1017/qua.2017.24 Published online by Cambridge University Press

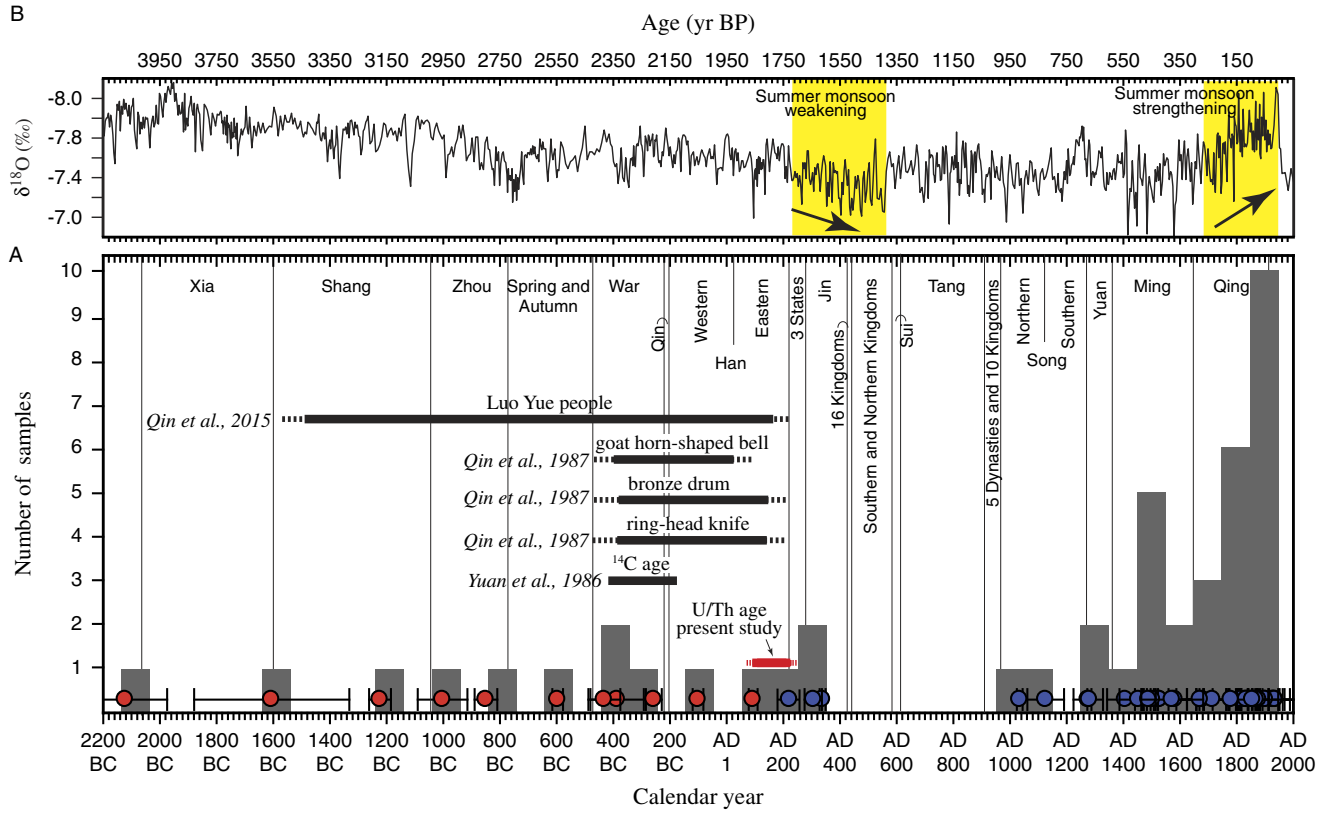

Figure 8. The age of the rock paintings at Mt. Huashan site. (A) Comparison of the present U/Th dating results with the previous age estimates by ^{14}C ages (Yuan et al., 1986) and that inferred from iconographical studies (Qin et al., 1987). The red dots represent the U/Th ages for the samples underlying the paintings, the blue dots are the ages for the samples overlying the paintings, and the gray bars correspond to the number of analyzed samples sorted by their U/Th ages. (B) Stalagmite δ^{18}O record of East Asian monsoon intensity variation (Wang et al., 2005). (For interpretation of the references to color in this figure legend, the reader is referred to the web version of this article.)

method. This study does not exclude the possibility of older rock paintings existing at other sites in the Zuojiang River valley. Thus, further numerical dating research on the rock paintings in this valley is warranted.

ACKNOWLEDGMENTS

This research was carried out in the framework of the application for World Heritage for the "Zuojiang Huashan Rock Art Cultural Landscape" organized by the Guangxi Zhuang Autonomous Region Department of Culture. We thank Lan Ri-Yong, Zhou Han-Cheng, and Hu Peng-Cheng for their help in the field with sampling. We thank Eric Douville and François Thil for their help on the development of U/Th dating techniques at NNU. We thank Jeff Pigati and two anonymous reviewers, who provided insightful comments/suggestions to improve this paper. This research was supported partly by the National Natural Science Foundation of China (grant 41302136) and the China Postdoctoral Science Foundation (grant 2013M530263).

Supplementary material

To view supplementary material for this article, please visit https://doi.org/10.1017/qua.2017.24

REFERENCES

Aubert, M., Brumm, A., Ramli, M., Sutikna, T., Saptomo, E.W., Hakim, B., Morwood, M.J., van den Bergh, G.D., Kinsley, L., Dosseto, A., 2014. Pleistocene cave art from Sulawesi, Indonesia. *Nature* 514, 223–227.

Aubert, M., O'Connor, S., McCulloch, M., Mortimer, G., Watchman, A., Richer-LaFleche, M., 2007. Uranium-series dating rock art in East Timor. *Journal of Archaeological Science* 34, 991–996.

Ayalon, A., Bar-Matthews, M., Kaufman, A., 1999. Petrography, strontium, barium and uranium concentrations, and strontium and uranium isotope ratios in speleothems as palaeoclimatic proxies: Soreq Cave, Israel. *Holocene* 9, 715–722.

Bednarik, R., Li, F., 1991. Rock art dating in China: past and future. *Artefact* 14, 25–33.

Cheng, H., Edwards, R.L., Shen, C.-C., Polyak, V.J., Asmerom, Y., Woodhead, J., Hellstrom, J., *et al.*, 2013. Improvements in ^{230}Th dating, ^{230}Th and ^{234}U half-life values, and U–Th isotopic measurements by multi-collector inductively coupled plasma mass spectroscopy. *Earth and Planetary Science Letters* 371–372, 82–91.

Cole, N., Watchman, A., 2005. AMS dating of rock art in the Laura Region, Cape York Peninsula, Australia – protocols and results of recent research. *Antiquity* 79, 661–678.

Corchón, M.S., Garate, D., Rivero, O., Valladas, H., Pons-Branchu, E., Murelaga, X., Ortega, P., Vicente, F.J., 2015. U-series and ^{14}C dating for a newly discovered decorated area in the paleolithic cave of la Pena de Candamo (Asturies, Northern Spain). *Journal of Archaeological Science: Reports* 3, 371–380.

David, B., Barker, B., Petchey, F., Delannoy, J.-J., Geneste, J.-M., Rowe, C., Eccleston, M., Lamb, L., Whear, R., 2013. A 28,000 year old excavated painted rock from Nawarla Gabarnmang, northern Australia. *Journal of Archaeological Science* 40, 2493–2501.

Douville, E., Salle, E., Frank, N., Eisele, M., Pons-Branchu, E., Ayrault, S., 2010. Rapid and accurate U-Th dating of ancient carbonates using inductively coupled plasma-quadrupole mass spectrometry. *Chemical Geology* 272, 1–11.

Fontugne, M., Shao, Q., Frank, N., Thil, F., Guidon, N., Boeda, E., 2013. Cross-dating (Th/U-^{14}C) of calcite covering prehistoric paintings at Serra da Capivara National Park, Piaui, Brazil. *Radiocarbon* 55, 1191–1198.

Ford, D.C., Williams, P.W., 2007. Karst Hydrogeology and Geomorphology. John Wiley and Sons, Chichester, UK.

Garcia-Diez, M., Hoffmann, D.L., Zilhao, J., de las Heras, C., Lasheras, J.A., Montes, R., Pike, A.W.G., 2013. Uranium series dating reveals a long sequence of rock art at Altamira Cave (Santillana del Mar, Cantabria). *Journal of Archaeological Science* 40, 4098–4106.

Garnett, E.R., Andrews, J.E., Preece, R.C., Dennis, P.F., 2004. Climate change recorded by stable isotopes and trace elements in a British Holocene tufa. *Journal of Quaternary Science* 19, 251–262.

Genty, D., Massault, M., Gilmour, M., Baker, A., Verheyden, S., Keppens, E., 1999. Calculation of past dead carbon proportion and variability by the comparison of AMS ^{14}C and TIMS U/Th ages on two Holocene stalagmites. *Radiocarbon* 41, 251–270.

Göktürk, O.M., Fleitmann, D., Badertscher, S., Cheng, H., Edwards, R.L., Leuenberger, M, Fankhauser, A., Tüysük, O., Kramers, J., 2011. Climate on the southern Black Sea coast during the Holocene: implications from the Sofular Cave record. *Quaternary Science Reviews* 30, 2433–2445.

Goslar, T., Hercman, H., Pazdur, A., 2000. Comparison of U-series and radiocarbon dates of speleothems. *Radiocarbon* 42, 403–414.

Guo, H., Han, R., Huang, H., Lan, R., Xie, R., 2010. Types of weathering of the Huashan rock paintings. In Agnew, N. (Ed.), Conservation of Ancient Sites on the Silk Road: Proceedings of the Second International Conference on Conservation of Grotto Sites, Mogao Grottoes, Dunhuang, People's Republic of China, June 28–July 3, 2004. Getty Conservation Institute, Los Angeles, pp. 311–315.

Hellstrom, J., Pickering, R., 2015. Recent advances and future prospects of the U-Th and U-Pb chronometers applicable to archaeology. *Journal of Archaeological Science* 56, 32–40.

Hellstrom, J.C., McCulloch, M.T., 2000. Multi-proxy constraints on the climatic significance of trace element records from a New Zealand speleothem. *Earth and Planetary Science Letters* 179, 287–297.

Hiess, J., Condon, D.J., McLean, N., Noble, S.R., 2012. $^{238}U/^{235}U$ systematics in terrestrial uranium-bearing minerals. *Science* 335, 1610–1614.

Holmgren, K., Lauritzen, S.-E., Possnert, G., 1994. $^{230}Th^{234}U$ and ^{14}C dating of a late Pleistocene stalagmite in Lobatse II Cave, Botswana. *Quaternary Science Reviews* 13, 111–119.

Ihlenfeld, C., Norman, M.D., Gagan, M.K., Drysdale, R.N., Maas, R., Webb, J., 2003. Climatic significance of seasonal trace element and stable isotope variations in a modern freshwater tufa. *Geochimica et Cosmochimica Acta* 67, 2341–2357.

Kaufman, A., Wasserburg, G.J., Porcelli, D., Bar-Matthews, M., Ayalon, A., Halicz, L., 1998. U-Th isotope systematics from the Soreq cave, Israel and climatic correlations. *Earth and Planetary Science Letters* 156, 141–155.

Lachniet, M.S., Bernal, J.B., Asmerom, Y., Polyak, V., 2012. Uranium loss and aragonite–calcite age discordance in a calcitized aragonite stalagmite. *Quaternary Geochronology* 14, 26–37.

Lojen, S., Trkov, A., Scancar, J., Vazquez-Navarro, J.-A., Cukrov, N., 2009. Continuous 60-year stable isotopic and earth-alkali element records in a modern laminated tufa (Jaruga, river Krka, Croatia): implications for climate reconstruction. *Chemical Geology* 258, 242–250.

Maher, K., Ibarra, D.E., Oster, J.L., Miller, D.M., Redwine, J.L., Reheis, M.C., Harden, J.W., 2014. Uranium isotopes in soils as a proxy for past infiltration and precipitation across the western United States. *American Journal of Science* 314, 821–857.

McDermott, F., Frisia, S., Huang, Y., Longinelli, A., Spiro, B., Heaton, T.H.E., Hawkesworth, C.J., *et al*., 1999. Holocene climate variability in Europe: evidence from $\delta^{18}O$, textural and extension-rate variations in three speleothems. *Quaternary Science Reviews* 18, 1021–1038.

McMillan, E.A., Fairchild, I.J., Frisia, S., Borsato, A., McDermott, F., 2005. Annual trace element cycles in calcite–aragonite speleothems: evidence of drought in the western Mediterranean 1200–1100 yr BP. *Journal of Quaternary Science* 20, 423–433.

Morwood, M.J., Walsh, G.L., Watchman, A.L., 2010. AMS radiocarbon ages for beeswax and charcoal pigments in north Kimberley rock art. *Rock Art Research* 27, 3–8.

Noronha, A.L., Johnson, K.R., Hu, C., Ruan, J., Southon, J.R., Ferguson, J.E., 2014. Assessing influences on speleothem dead carbon variability over the Holocene: implications for speleothem-based radiocarbon calibration. *Earth and Planetary Science Letters* 394, 20–29.

Ortega, R., Maire, R., Deve, G., Quinif, Y., 2005. High-resolution mapping of uranium and other trace elements in recrystallized aragonite–calcite speleothems from caves in the Pyrenees (France): implication for U-series dating. *Earth and Planetary Science Letters* 237, 911–923.

Pike, A.W.G., Gilmour, M., Pettitt, P., Jacobi, R., Ripoll, S., Bahn, P., Munoz, F., 2005. Verification of the age of the palaeolithic cave art at Creswell Crags, UK. *Journal of Archaeological Science* 32, 1649–1655.

Pike, A.W.G., Hoffmann, D.L., Garcia-Diez, M., Pettitt, P.B., Alcolea, J., De Balbin, R., Gonzalez-Sainz, C., *et al*., 2012. U-series dating of paleolithic art in 11 caves in Spain. *Science* 336, 1409–1413.

Plagnes, V., Causse, C., Fontugne, M., Valladas, H., Chazine, J.-M., Fage, L.-H., 2003. Cross dating (Th/U-^{14}C) of calcite covering prehistoric paintings in Borneo. *Quaternary Research* 60, 172–179.

Pons-Branchu, E., Bourrillon, R., Conkey, M., Fontugne, M., Fritz, C., Gárate, D., Quiles, A., *et al*., 2014a. U-series dating of carbonate formations overlying paleolithic art: interest and limitations. *Bulletin de la Société Préhistorique Française* 111, 211–224.

Pons-Branchu, E., Douville, E., Roy-Barman, M., Dumont, E., Branchu, P., Thil, F., Frank, N., Bordier, L., Borst, W., 2014b. A geochemical perspective on Parisian urban history based on U–Th dating, laminae counting and yttrium and REE concentrations of recent carbonates in underground aqueducts. *Quaternary Geochronology* 24, 44–53.

https://doi.org/10.1017/qua.2017.24 Published online by Cambridge University Press

Qin, C.L., Fu, G.H., Qin, L.D., 2015. One century of the Luo Yue cultural studies (part 1). [In Chinese.] *Guangxi Ethnic Research* 124, 90–97.

Qin, S.M., Qin, C.L., Lu, M.F., Yu, R.Y., 1987. The Investigation and Study of the Rock Art of the Zuojiang River Valley in Guangxi. [In Chinese.]. Guangxi Ethnic Printing House, Nanning, China.

Quiles, A., Valladas, H., Bocherens, H., Delque-Kolic, E., Kaltnecker, E., van der Plicht, J., Delannoy, J.-J., *et al*., 2016. A high-precision chronological model for the decorated Upper Paleolithic cave of Chauvet-Pont d'arc, Ardeche, France. *Proceedings of the National Academy of Sciences of the United States of America* 113, 4670–4675.

Railsback, B.L., Dabous, A.A., Osmond, J.K., Fleisher, C.J., 2002. Petrographic and geochemical screening of speleothems for U-series dating: an example from recrystallized speleothems from Wadi Sannur Cavern, Egypt. *Journal of Cave and Karst Studies* 64, 108–116.

Ramsey, C.B., 2009. Bayesian analysis of radiocarbon dates. *Radiocarbon* 51, 337–360.

Reimer, P.J., Bard, E., Bayliss, A., Beck, J.W., Blackwell, P.G., Bronk Ramsey, C., Buck, C.E., *et al*., 2013. IntCal 13 and Marine13 radiocarbon age calibration curves 0–50,000 years cal BP. *Radiocarbon* 55, 1869–1887.

Robinson, L.F., Henderson, G.M., Hall, L., Matthews, I., 2004. Climatic control of riverine and seawater uranium-isotope ratios. *Science* 305, 851–854.

Russ, J., Hyman, M., Shafer, H.J., Rowe, M.W., 1990. Radiocarbon dating of prehistoric rock paintings by selective oxidation of organic carbon. *Nature* 348, 710–711.

Russell, W.A., Papanastassiou, D.A., Tombrello, T.A., 1978. Ca isotope fractionation on the Earth and other solar system materials. *Geochimica et Cosmochimica Acta* 42, 1075–1090.

Smith, M.A., Watchman, A., Ross, J., 2009. Direct dating indicates a Mid-Holocene age for archaic rock engravings in arid central Australia. *Geoarchaeology* 24, 191–203.

Steelman, K.L., Rowe, M.W., Shirokov, V.N., Southon, J.R., 2002. Radiocarbon dates for pictographs in Ignatievskaya Cave, Russia: Holocene age for supposed Pleistocene fauna. *Antiquity* 76, 341–348.

Stuiver, M., Polach, H.A., 1977. Discussion: reporting of ^{14}C data. *Radiocarbon* 19, 355–363.

Taçon, P.S.C., Aubert, M., Gang, L., Decong, Y., Hong, L., May, S.K., Fallon, S., Ji, X.P., Curnoe, D., Herries, A.I.R., 2012. Uranium-series age estimates for rock art in southwest China. *Journal of Archaeological Science* 39, 492–499.

Tisnérat-Laborde, N., Poupeau, J.J., Tannau, J.F., Paterne, M., 2001. Development of a semi-automated system for routine preparation of carbonate samples. *Radiocarbon* 43, 299–304.

Valladas, H., Cachier, H., Arnold, M., 1990. AMS C-14 dates for the prehistoric Cougnac cave paintings and related bone remains. *Rock Art Research* 7, 18–19.

Valladas, H., Cachier, H., Maurice, P., Bernaldo de Quirost, F., Clottes, J., Cabrera Valdés, V., Uzquiano, P., Arnold, M., 1992. Direct radiocarbon dates for prehistoric paintings at the Altamira, El Castillo and Niaux caves. *Nature* 357, 68–70.

Valladas, H., Clottes, J., Geneste, J.M., Garcia, M.A., Arnold, M., Cachier, H., Tisnerat-Laborde, N., 2001. Palaeolithic paintings: evolution of prehistoric cave art. *Nature* 413, 479.

Veizer, J., Ala, D., Azmy, K., Bruckschen, P., Buhl, D., Bruhn, F., Carden, G.A.F., *et al*., 1999. $^{87}Sr/^{86}Sr$, $\delta^{13}C$ and $\delta^{18}O$ evolution of Phanerozoic seawater. *Chemical Geology* 161, 59–88.

Wang, N.S., 1984. An introduction to rock paintings in Yunnan Province (People's Republic of China). *Rock Art Research* 1, 75–90.

Wang, Y., Cheng, H., Edwards, R.L., He, Y., Kong, X., An, Z., Wu, J., Kelly, M.J., Dykoski, C.A., Li, X., 2005. The Holocene Asian monsoon: links to solar changes and North Atlantic climate. *Science* 308, 854–857.

Watchman, A.L., 1993. Evidence of a 25,000-year-old pictograph in northern Australia. *Geoarchaeology* 8, 465–473.

White, W.B., 1988. *Geomorphology and Hydrology of Karst Terrains*. Oxford University Press, New York.

Woo, K.S., Choi, D.W., 2006. Calcitization of aragonite speleothems in limestone caves in Korea: diagenetic process in a semiclosed system. *Geological Society of America, Special Papers* 404, 297–306.

Yang, B., Braeuning, A., Johnson, K.R., Shi, Y., 2002. General characteristics of temperature variation in China during the last two millennia. *Geophysical Research Letter* 29, 1324. http://dx.doi.org/10.1029/2001GL014485.

Yuan, S.X., Chen, T.M., Hu, Y.Q., 1986. ^{14}C ages for the rock paintings at Huashan Mountain, Ningming, Guangxi. [In Chinese.] *Guangxi Ethnic Research* 4, 27–33.

Zhang, H.W., Cai, Y.J., Tan, L.C., Qin, S.J., An, Z.S., 2014. Stable isotope composition alteration produced by the aragonite-to-calcite transformation in speleothems and implications for paleoclimate reconstructions. *Sedimentary Geology* 309, 1–14.

Zhou, J., Lundstrom, C.C., Fouke, B., Panno, S., Hackley, K., Curry, B., 2005. Geochemistry of speleothem records from southern Illinois: development of (^{234} U)/(^{238}U) as a proxy for paleoprecipitation. *Chemical Geology* 221, 1–20.

https://doi.org/10.1017/qua.2017.24 Published online by Cambridge University Press